GDCh

Research Articles

Angewandte
Chemie
International Edition
www.angewandte.org

Photosensitizers

Using Biological Photophysics to Map the Excited-State Topology of Molecular Photosensitizers for Photodynamic Therapy

Avinash Chettri, Tingxiang Yang, Houston D. Cole, Ge Shi, Colin G. Cameron, Sherri A. McFarland,* and Benjamin Dietzek-Ivanšić*

Abstract: This study employs TLD1433, a Ru^{II}-based photodynamic therapy (PDT) agent in human clinical trials, as a benchmark to establish protocols for studying the excited-state dynamics of photosensitizers (PSs) *in cellulo*, in the local environment provided by human cancer cells. Very little is known about the excited-state properties of any PS in live cells, and for TLD1433, it is *terra incognita*. This contribution targets a general problem in phototherapy, which is how to interrogate the light-triggered, function-determining processes of the PSs in the relevant biological environment, and establishes methodological advances to study the ultrafast photoinduced processes for TLD1433 when taken up by MCF7 cells. We generalize the methodological developments and results in terms of molecular physics by applying them to TLD1433's analogue TLD1633, making this study a benchmark to investigate the excited-state dynamics of phototoxic compounds in the complex biological environment.

Introduction

TLD1433 (or [Ru(4,4′-dmb)$_2$(IP-3T)](Cl)$_2$ [where: 4,4′-dmb = 4,4′-dimethyl-2,2′-bipyridine; IP = imidazo[4,5-*f*]-[1,10]phenanthroline; 3T = α-terthiophene]), a Ru^{II} complex incorporating the 1*H*-imidazo[4,5-*f*][1,10]phenanthroline ligand appended with α-terthiophene (Scheme 1), is the first Ru photosensitizer (PS) to enter clinical trials.[1] TLD1433 is currently in a Phase II study (ClinicalTrials.gov identifier: NCT03945162) for treating nonmuscle-invasive bladder cancer with photodynamic therapy (PDT), a method of selectively destroying tumors via PS-mediated sensitization of reactive molecular species (RMS).[2] For TLD143 a long-lived triplet intraligand charge transfer (^{3}ILCT) excited state that sensitizes singlet oxygen (^{1}O$_2$), and potentially other RMS, in high yield has been implicated in its photocytotoxicity based on computational[3] and cell-free solution

studies.[4] In vitro PDT effects for TLD1433 have been quantified with phototherapeutic indices (PIs) exceeding 10^3 for a variety of human cancer cell lines,[1a,b,5] and even $> 10^2$ in cell lines such as MCF7 (Figure 1a). Despite the extensive photophysical studies in solution, the photocytotoxicity studies using human cancer cells, and the critical preclinical in vivo studies that led to human clinical trials, nothing is known about the excited-state topology of this benchmark Ru PS in human cells despite the fact that such light-driven elementary photoprocesses are key to a comprehensive understanding of the biomolecular and clinical function of the complex.

This lack of information pertaining to *biological photophysics* is not unique to TLD1433. The excited-state dynamics of photoactive molecules in the cellular environment remain largely unexplored, despite luminescence spectroscopy and microscopy being commonly used to probe intracellular ions and molecules as well as parameters such as pH, local viscosity, and viability.[6] The impact of the specific local environment of human cells has not been interrogated with respect to the upper excited states of photocytotoxic compounds. To fill this gap, we established an experimental methodology that uses transient absorption (TA) spectroscopy and microscopy to study the sub-ns excited-state dynamics of photocytotoxic complexes *in cellulo*. Such investigations pose many challenges, including the

[*] A. Chettri, T. Yang, Prof. Dr. B. Dietzek-Ivanšić
Department Functional Interfaces, Leibniz-Institute of Photonic Technology Jena
Albert-Einstein-Straße 9, 07745 Jena (Germany)
and
Institute of Physical Chemistry, Friedrich-Schiller University Jena
Helmholtzweg 4, 07743 Jena (Germany)
E-mail: benjamin.dietzek@leibniz-ipht.de

H. D. Cole, G. Shi, Dr. C. G. Cameron, Prof. Dr. S. A. McFarland
Department of Chemistry and Biochemistry, The University of Texas at Arlington
Arlington, TX-76019 (USA)
E-mail: sherri.mcfarland@uta.edu
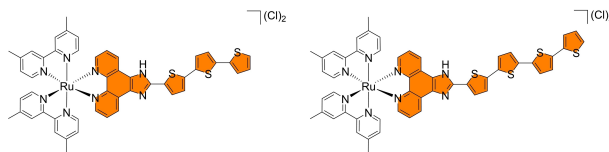
Scheme 1. Molecular structures of TLD1433, [Ru(4,4′-dmb)$_2$(IP-3T)](Cl)$_2$ (Ru-ip-3T), and TLD1633, [Ru(4,4′-dmb)$_2$(IP-4T)](Cl)$_2$ (Ru-ip-4T).
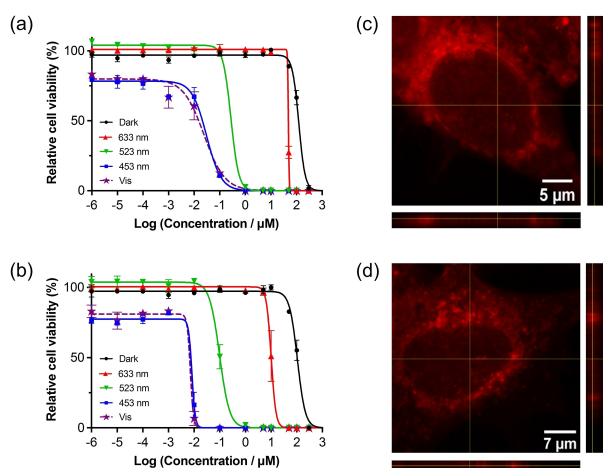
Figure 1. (Photo)cytotoxic effects on MCF7 cells dosed with a) Ru-ip-3T or b) Ru-ip-4T. Light treatments were 100 J cm^{-2} broadband visible (400–700 nm) or monochromatic light delivered at a rate of ~28 mW·cm^{-2} with a DLI of 16 h. Localization of c) Ru-ip-3T and d) Ru-ip-4T in fixed MCF7 cells after 16 h incubation visualized by confocal emission microscopy ($\lambda_{ex.} = 450$ nm, $\lambda_{em.} > 570$ nm). Images were collected from different focal planes along the z axis to ensure intracellular PS was probed.

the cellular environment to bridge the gap between photophysical studies in solution and phototoxicity assessment in human cancer cells (Scheme 2). Wide-field (i.e., without spatial resolution) sub-ns TA spectroscopy is used to study the excited-state relaxation kinetics of the PS in live cells over the first several ns following photon absorption. Complementary luminescence microscopy is used to obtain information on the PS distribution in these cells, which guides the TA microscopy analysis on PS-treated fixed cells. This static cellular environment is advantageous for the TA microscopy experiment where the sample experiences a much higher photon flux over a smaller area. We use TLD1433 and its close relative TLD1633 (or [Ru(4,4′-dmb)$_2$(IP-4T)](Cl)$_2$ [where: 4T = α-quaterthiophene]) (Scheme 1) to demonstrate our approach in human MCF7 breast cancer cells, which yields unprecedented insights regarding non thermalized excited-state processes for these phototherapy agents. The robust nature of MCF7 cells, particularly their ability to be easily cultured, makes it the ideal cell line of choice for our investigation. Our new experimental methodology for biological photophysics provides a benchmark for deciphering the excited-state dynamics to facilitate the rational design of improved PDT agents.

fact that the light exposure central to optical spectroscopy activates the PS to form RMS and cellular damage during the course of the experiment. The highly dynamic nature of the living cellular environment is exacerbated by its real-time response to phototoxic stressors.

Our methodology builds on spectroscopic studies of photocytotoxic compounds in organic solvents and more complex solutions containing biomolecules,[4c, 7] microscopy studies characterizing long-lived emissive states of transition metal complexes in cells,[8] and more specialized TA microscopy techniques focused on biomedical diagnostics or photophysics in fixed cells.[9] Herein we focus specifically on interrogating the topology of electronically excited states in

Results and Discussion

Live Cell TA Spectroscopy

MCF7 cells were incubated with 40 µM Ru-ip-3T or Ru-ip-4T for 16 h prior to recording the live cell kinetics. The selected concentration of 40 µM produced the characteristic signature observed for the build-up of the oligothienyl-localized triplet at 660 nm in solution (Figure S1) with acceptable signal-to-noise ratio without any dark cytotoxicity (Figure 1a and b). The viability of cells treated with 40 µM PS was confirmed by the absence of Trypan Blue staining. PS uptake into the cytosol was confirmed by
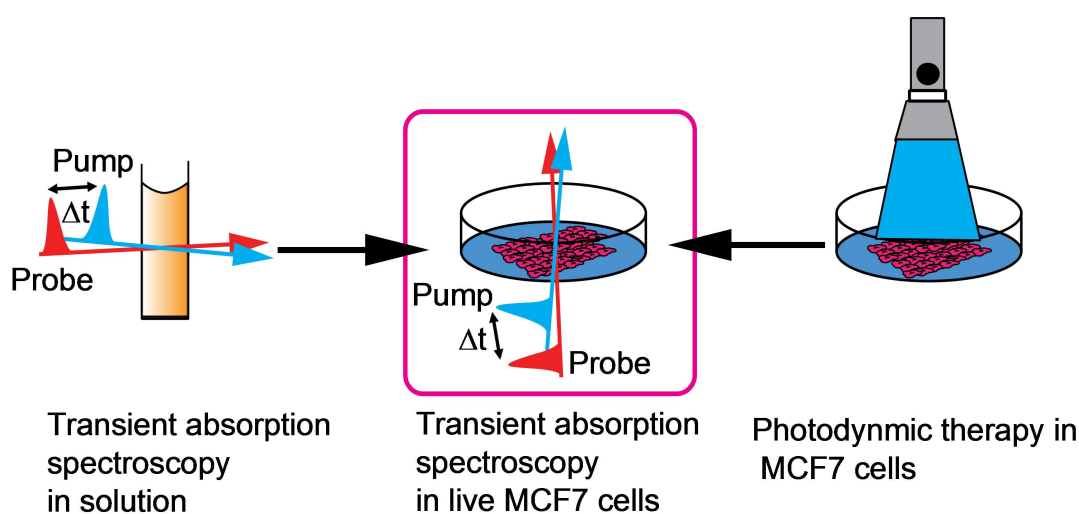
Scheme 2. New methodology bridges the gap between time-resolved spectroscopy to study excited-state dynamics in solution and phototoxicity evaluation in cellular assays.

confocal microscopy via emission >570 nm in fixed cells (Figure 1c and d) and corroborated with TA microscopy (see below). Because the signal integration time is quite long for TA microscopy, we use it to image the PS based on its excited-state absorption rather than to obtain spectroscopic information about the PS in selected positions within the live cells.

Live cell TA spectroscopy of Ru-ip-3T. Measuring excited-state kinetics for PSs in cells poses a challenge in that the excitation pulse activates the PS to form RMS, which changes the cellular environment during the experiment. The intensities of the pump pulses as well as the overall scan time influence the state of the cell with regard to various stages toward RMS-induced cell death, exacerbating the already-dynamic cellular environment experienced by the PS. To probe the earliest stage where the largest number of cells are viable, it is best to minimize the number of photons incident on the sample. MCF7 cells tolerated a 2-min train of pump pulses at a power of 20 µW with no evidence of cell death as confirmed by the absence of Trypan Blue staining (Figure S2). This total exposure time was reduced to 30 s for cells treated with Ru-ip-3T to avoid cell death triggered by PS activation with the pump pulse with longer exposure times (Figure 2c and Figure S3). The individual pump-probe pulse pairs recorded at a given pump-probe delay were limited to 200, and the point density on the delay-time axis was limited to 30 for recording a single transient. The pump power did not exceed 20 µW. To put these numbers in perspective, a typical femtosecond TA scan on photostable molecules in cell-free solution takes

about 10 min, with pump-power reaching 100 µW, where each individual scan contains about 600 pulse-pairs per delay time and about 200 delay times per experimental scan (Figure 2a).

The kinetic profile of Ru-ip-3T (40 µM) in living MCF7 cells was measured using a set-up built in house,[10] which consists of a modified TA system that directs the laser pulses vertically with respect to the optical table. Petri dishes containing the cells dosed with PS are mounted in the sample stage positioned in the focal plane of the laser pulses. Sample excitation was delivered at 400 nm to populate ^{1}MLCT and ^{1}ILCT states, which ultimately relax to lower-lying and function-determining ^{3}ILCT states that exhibit a prominent ESA near 650 nm in water (Figure 2a). These states, which are localized to the oligothienyl unit, are key for ROS generation and hence the photocytotoxicity of the complexes.[4] Therefore, the probe wavelength was set to 650 nm for the live cell TA spectroscopy.

The TA kinetics at 650 nm reflect a pulse-width limited rise of the differential absorption signal followed by a slower increase. This bi-exponential increase is complete within the first 85 ps following photoexcitation and is characterized by time constants $\tau_1^{rise} = 1.5$ ps and $\tau_2^{rise} = 13$ ps (Figure 2b). We associate the biexponential increase observed in live cells with fast internal conversion from vibrationally hot ^{3}MLCT states to hot ^{3}ILCT states (τ_1^{rise}) followed by vibrational relaxation within the ^{3}ILCT manifold (τ_2^{rise}, Figure 2d).[4a] This assignment is based on the assumption that the ESA signal from the cool ^{3}ILCT state with its planarized conjugated ligand is much stronger than that of the hot
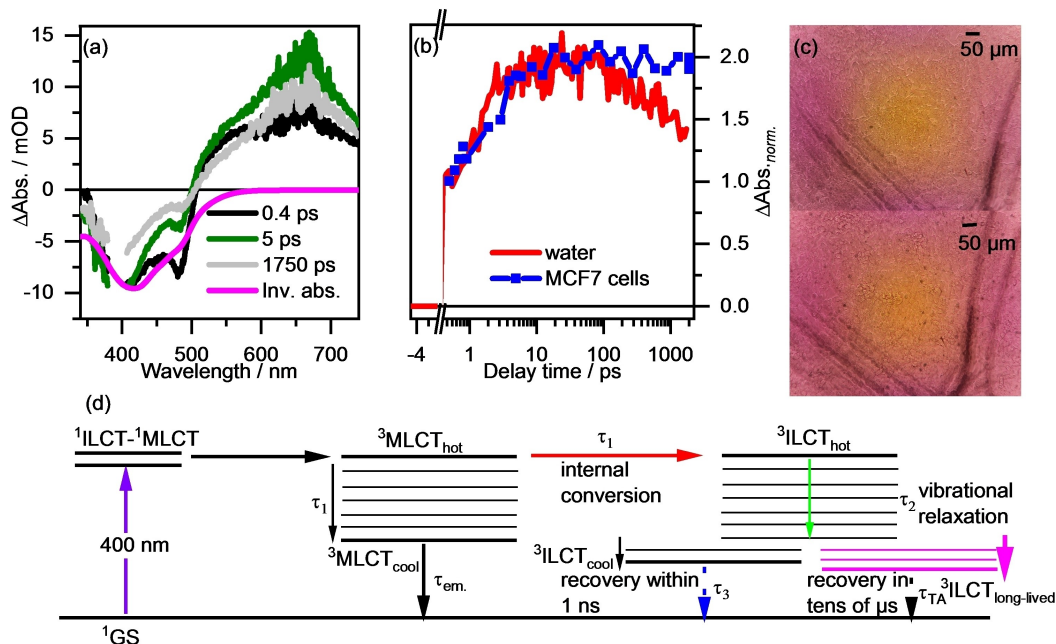

Figure 2. a) Femtosecond TA spectra collected for Ru-ip-3T at 40 µM in water with $\lambda_{ex.} = 400$ nm; inverted absorption spectrum indicated in pink. b) TA kinetics for Ru-ip-3T at 40 µM in water or in MCF7 cells after 16 h incubation ($\lambda_{ex.} = 400$ nm, $\lambda_{probe} = 650$ nm). c) Bright-field microscope images (10x) of MCF7 cells dosed with Ru-ip-3T and incubated for 16 h before and after irradiation with $\lambda_{ex.} = 400$ nm for 30 s. The absence of Trypan Blue staining after irradiation was used to confirm live cells. d) Jablonski diagram showing the photophysical model for Ru-ip-3T and Ru-ip-4T in water with $\lambda_{ex.} = 400$ nm.[4a] The long-lived function determining ^{3}ILCT state (emphasized in pink) is responsible for phototoxicity of Ru-ip-3T and Ru-ip-4T.[4b]

³ILCT state. Beyond 100 ps, the signal is relatively constant within the experimentally accessible delay-time window of 1.9 ns. These kinetics within MCF7 cells resemble the corresponding TA kinetics measured for highly concentrated Ru-ip-3T in water (500 µM, Figure S4), and both differ notably from the kinetics recorded for lower concentrations of Ru-ip-3T in water (40 µM, Figure 2b). When MCF7 cells are dosed with 40 µM Ru-ip-3T, there is no decay of the long-lived ³ILCT state over the 1.9 ns window whereas the same concentration of the PS in water yields a slow decay corresponding to a 35 % decrease of the signal (Figure 2b). To account for this finding, which is reminiscent of the excited-state relaxation of Ru-ip-3T when interacting with calf thymus DNA in solution,[4c] we suggest that intermolecular interactions modulate the slower excited-state kinetics such as intracellular self-association due to high local concentrations or binding to biological macromolecules.[4c] Both scenarios would be expected to result in reduced structural flexibility of the terthienyl chain that may prolong the lifetime of the ³ILCT state. This finding is mechanistically important as the ³ILCT state is the major contributor to ROS formation and prolongation of its lifetime in live cells likely enhances phototoxicity.

Live cell TA spectroscopy of Ru-ip-4T. The light exposure for cells dosed with Ru-ip-4T, a more potent PS, had to be reduced further for the analysis because Ru-ip-4T renders the MCF7 cells non-viable after a scan time of only 30 s (Figure S3) using the pulse conditions applied during the TA experiment for Ru-ip-3T in live cells. However, decreasing the pump-intensity or the number of pulse-pairs per delay time reduced the signal-to-noise ratio and made interpretation of the kinetics impossible. To address this, irradiation was limited to 10 s (Figure 3a) and the petri dish containing the treated cells was repositioned during the TA experiment to ensure that only a fraction of the overall differential absorption kinetics was recorded at each sample position. The overall differential absorption kinetics spanning the range of the experimentally accessible delay times was then reconstructed from the individual segments, each normalized to the onset signal of the next segment (Figure 3b). The delay time segments were: 0–5, 5–15, 15–500, and 500–1800 ps. Stitching the kinetics by position and delay time in this manner assumes that the photophysics of the molecular and cellular ensemble that is sampled is independent of the position of the laser focus. Admittedly, with higher spatial resolution, this would not be possible.

The resulting kinetics recorded at 680 nm, the ESA maximum for Ru-ip-4T, is reminiscent of the kinetics measured for Ru-ip-3T (see above). The signal at 680 nm increases up to 100 ps and then remains constant within the experimentally accessible delay time range of 1.9 ns (Figure 4c). The increase can be fit to a biexponential ($\tau_1^{rise} = 1$ ps and $\tau_2^{rise} = 7.5$ ps) and, as for Ru-ip-3T, reflects the formation of hot ³ILCT states (from hot ³MLCT states) followed by relaxation within the ³ILCT manifold to yield the long-lived ³ILCT state that has key functional relevance. These time constants are similar to what was observed for highly concentrated aqueous solution (500 µM, Figure 3c and S5), and differ markedly from those measured in dilute
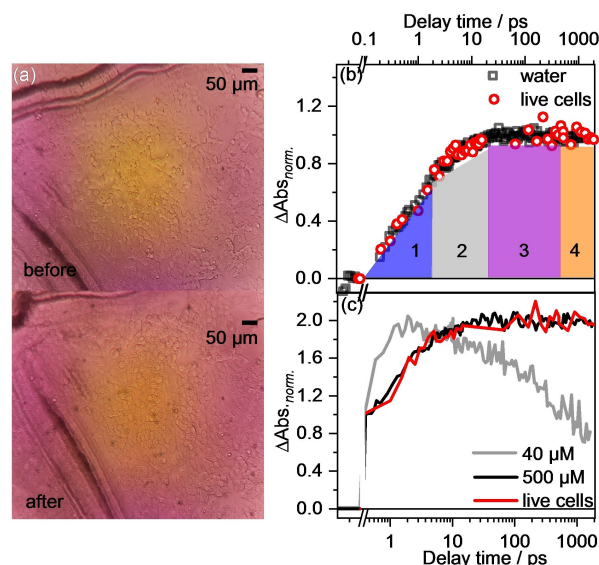

Figure 3. a) Bright-field microscope images (10x) of MCF7 cells dosed with 40 µM Ru-ip-4T before and after irradiation with $\lambda_{ex.} = 400$ nm for 10 s. The absence of Trypan Blue staining after irradiation confirmed live cells. b) Collection points (point density) in the kinetic traces of Ru-ip-4T in MCF7 cells compared to water. The colored areas labeled 1–4 represent segments of the overall reconstructed signal collected from four different positions in the petri dish containing MCF7 cells. c) Kinetics for Ru-ip-4T in MCF7 cells at 40 µM compared to 40 µM and 500 µM PS in water with $\lambda_{ex.} = 400$ nm; $\lambda_{probe} = 680$ nm

aqueous solution (40 µM in water, Figure S6) where the long-lived ³ILCT state undergoes decay within the 1.9 ns time window (Figure 3c). As for Ru-ip-3T we attribute this difference for Ru-ip-4T to the reduced flexibility of the oligothiophene chain upon self-association (e.g., high concentration) or associated with biological targets (e.g., in live cells). Conformational restriction is known to limit non-radiative decay of excited states,[11] prolonging the ³ILCT lifetime in live cells, and appears to be a general feature of Ru-ip-3T and Ru-ip-4T.

TA Microscopy

TA spectroscopy yields insights regarding the effect of the confined and compact environment of the cell on the population and decay of the function-determining long-lived ³ILCT state for two different PSs of interest for PDT. However, the data obtained reflect dynamics that are averaged over many different cells and subcellular positions. Therefore, TA spectroscopy in live cells does not consider the influence of intracellular structural heterogeneity on the light-induced excited-state dynamics. We hypothesize that different local environments within human cells[12] will lead to different excited-state relaxation kinetics of molecules placed into those local environments. To begin exploring this hypothesis, MCF7 cells dosed with Ru-ip-3T were fixed and studied by TA microscopy[9,13] with a previously reported setup.[9] The pump and probe pulses were centered at 400 and 650 nm, respectively. Fixed cells were used to
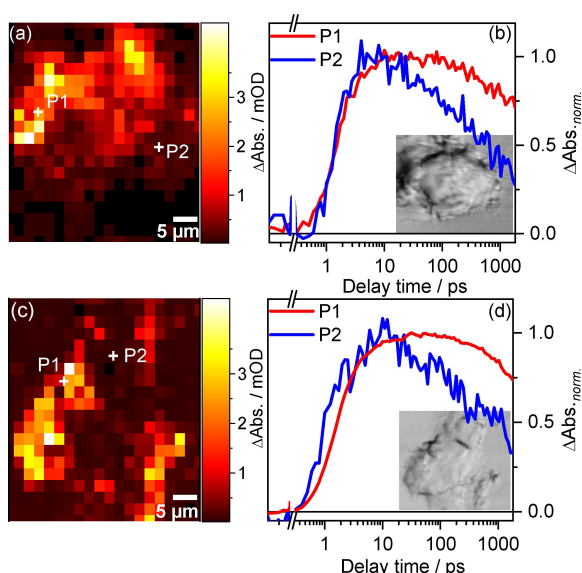
Figure 4. a) Distribution of Ru-ip-3T in MCF7 cells obtained by spatially-resolved TA microscopy. The heat map image was recorded with pump pulses centered at $\lambda_{ex.} = 400$ nm and probe pulses centered at $\lambda_{probe} = 650$ nm. The pump-probe delay was set to 5 ps. b) Normalized TA kinetic traces for Ru-ip-3T in MCF7 cells with $\lambda_{ex.} = 400$ nm and $\lambda_{probe} = 650$ nm. The individual kinetics were recorded at different focal positions within a fixed cell on a quartz slide. Inset shows the phase contrast image of the MCF7 cell depicted in (a). c) Distribution of Ru-ip-4T in MCF7 cells obtained by spatially-resolved TA microscopy with $\lambda_{ex.} = 400$ nm and $\lambda_{probe} = 680$ nm with the pump-probe delay set to 5 ps. d) Normalized TA kinetic traces for Ru-ip-4T in MCF7 cells with $\lambda_{ex.} = 400$ nm and $\lambda_{probe} = 680$ nm recorded at different focal positions. Inset shows the phase contrast image of the MCF7 depicted in (c).

probe the effect of different local environments in the absence of any time-dependent subcellular changes due to cell death pathways that would be triggered by Ru-ip-3T and Ru-ip-4T with the high photon flux of the TA microscope.

TA microscopy of Ru-ip-3T and Ru-ip-4T in MFC-7 cells. Figure 4a presents a TA map, where the TA signal (pump = 400 nm, probe at 650 nm, delay time 5 ps) is recorded at different positions of the cell. The size of each pixel in the TA map is 2.2 μm².

Although pixel sizes as small as 1.1 μm² can be obtained, 2.2 μm² was selected to reduce the scan time for each MCF7 cell during the experiment without any significant loss in resolution. The spatial fluctuations of the differential absorption signal for Ru-ip-3T, ranging from 0 to 3 mOD, demonstrate that subcellular heterogeneity influences the measurement. These data—and corresponding data recorded for MCF7 cells dosed with Ru-ip-4T (Figures 4a and c)—support the assertion that local environment causes local variations in the excited-state dynamics of the PS. The TA kinetics recorded for Ru-ip-3T in two different positions within the cytoplasm, P1 and P2, is shown in Figure 4b (additional points and their respective kinetics are shown in Figure S7). Assuming that the oscillator strengths of electronic transitions being probed do not change with environment (i.e., location in the MCF7 cell), P1 and P2 could

reflect positions of high and low local concentrations of Ru-ip-3T in the cytoplasm, respectively. Within the 1.8 ns time window, the TA kinetics at P1 and P2 are very different. At P1 there is a rise in the signal within 17 ps followed by a decay, whereas at P2 the signal rises within 5 ps and decays much faster compared to the signal at P1. While more systematic studies relating the specific local environment within the cells to the light-induced dynamics of the PS are required, already the results presented indicate that the photophysical behavior of Ru-ip-3T is sensitive to parameters such as local concentration and environment within the cytoplasm.

A similar experiment was performed for Ru-ip-4T in a fixed MCF7 cell with two positions in the cytoplasm, P1 and P2, selected as shown in Figure 4c (additional points and their respective kinetics are shown in Figure S8). An overall stronger signal is evident at P1 and is associated with a much slower decay compared to the comparably weaker signal at P2 that exhibits a prominent decay starting as early as 10 ps (Figure 4d). As for Ru-ip-3T, it appears that the variation in signal intensities as well as the decay kinetics at long delay times are most likely associated with different local concentrations and/or environments within the cytoplasm. While this remains to be independently verified, the assumption is in line with the concentration-dependent TA kinetics (see above), which show that higher concentrations of the PS and/or different environments slow the decay of the long-lived TA signal at 680 nm.

Conclusion

This report presents an experimental methodology, which allows the ultrafast light-induced dynamics of phototoxic molecules in living human cancer cells to be probed. The method was specifically designed to move us beyond photophysical studies of non-phototoxic molecules in human cells[14] to evaluating the excited-state topology of phototoxic molecules in living systems. Such studies were previously not possible but are critical to understanding in vitro photocytotoxicity since the intracellular photophysical dynamics are intimately linked to the function of PSs for PDT. We exemplify our approach of TA spectroscopy in live cells using two PSs, Ru-ip-3T and Ru-ip-4T. The data suggest that in the crowded environment of the cell, the structural flexibility of the extended ip-nT ligand is reduced, leading to a prolonged ³ILCT excited-state lifetime. While the data does not distinguish between intermolecular PS interactions and those between PS molecules and biological targets, it does confirm that *in cellulo* photophysical dynamics are very different from those in cell-free solution. Thus, to understand the key mechanistic aspects underlying the PS activity, it is imperative to study their photophysical properties and excited-state topologies *in cellulo*.

Conflict of Interest

S.A.M. has a potential research conflict of interest due to a financial interest with Theralase Technologies, Inc. and PhotoDynamic, Inc. A management plan has been created to preserve objectivity in research in accordance with UTA policy.

Data Availability Statement

The data that support the findings of this study are available from the corresponding authors upon reasonable request.

[1] a) G. Shi, S. Monro, R. Hennigar, J. Colpitts, J. Fong, K. Kasimova, H. Yin, R. DeCoste, C. Spencer, L. Chamberlain, A. Mandel, L. Lilge, S. A. McFarland, *Coord. Chem. Rev.* **2015**, *282*, 127–138; b) S. Monro, K. L. Colon, H. Yin, J. Roque III, P. Konda, S. Gujar, R. P. Thummel, L. Lilge, C. G. Cameron, S. A. McFarland, *Chem. Rev.* **2019**, *119*, 797–828; c) S. A. McFarland, A. Mandel, R. Dumoulin-White, G. Gasser, *Curr. Opin. Chem. Biol.* **2020**, *56*, 23–27; d) G. S. Kulkarni, L. Lilge, M. Nesbitt, R. J. Dumoulin-White, A. Mandel, M. A. Jewett, *Eur. Urol. Open Sci.* **2022**, *41*, 105–111.

[2] a) *Photodynamic Medicine: From Bench to Clinic* (Eds.: H. Kostron, T. Hasan), Royal Society Of Chemistry, London, **2016**; b) *Photodynamic Therapy: Basic Principles and Clinical Applications* (Eds.: B. W. Henderson, T. J. Dougherty), CRC, Boca Raton, **1992**; c) *Handbook of Photomedicine* (Eds.: M. R. Hamblin, Y. Huang), Taylor & Francis, New York, **2013**; d) *Advances in Photodynamic Therapy: Basic, Translational, and Clinical* (Eds.: M. R. Hamblin, P. Mróz), Artech House, Boston, **2008**; e) R. Bonnett, *Chemical Aspects of Photodynamic Therapy*, Gordon and Breach Science Publishers, Newark, **2000**.

[3] M. E. Alberto, J. Pirillo, N. Russo, C. Adamo, *Inorg. Chem.* **2016**, *55*, 11185–11192.

[4] a) A. Chettri, K. R. Schneider, H. D. Cole, J. A. Roque III, C. G. Cameron, S. A. McFarland, B. Dietzek, *J. Phys. Chem. A* **2021**, *125*, 6985–6994; b) A. Chettri, J. A. Roque III, K. R. Schneider, H. D. Cole, C. G. Cameron, S. A. McFarland, B. Dietzek, *ChemPhotoChem* **2021**, *5*, 421–425; c) A. Chettri, H. D. Cole, J. A. Roque III, K. R. Schneider, T. Yang, C. G. Cameron, S. A. McFarland, B. Dietzek-Ivanšić, *J. Phys. Chem. A* **2022**, *126*, 1336–1344.

[5] a) S.-K. Hsu, W.-T. Chang, I.-L. Lin, Y.-F. Chen, N. B. Padalwar, K.-C. Cheng, Y.-N. Teng, C.-H. Wang, C.-C. Chiu, *Cancers* **2020**, *12*, 2185; b) J. Fong, K. Kasimova, Y. Arenas, P. Kaspler, S. Lazic, A. Mandel, L. Lilge, *Photochem. Photobiol. Sci.* **2015**, *14*, 2014–2023; c) S. Chamberlain, H. D. Cole, J. Roque III, D. Bellnier, S. A. McFarland, G. Shafirstein, *Pharmaceuticals* **2020**, *13*, 137.

[6] a) H. K. Saeed, S. Sreedharan, P. J. Jarman, S. A. Archer, S. D. Fairbanks, S. P. Foxon, A. J. Auty, D. Chekulaev, T. Keane, A. J. H. M. Meijer, J. A. Weinstein, C. G. W. Smythe, J. Bernardino De La Serna, J. A. Thomas, *J. Am. Chem. Soc.* **2019**, *141*, 1101–1111; b) M. R. Gill, J. Garcia-Lara, S. J. Foster, C. Smythe, G. Battaglia, J. A. Thomas, *Nat. Chem.* **2009**, *1*, 662–667; c) M. R. Gill, D. Cecchin, M. G. Walker, R. S. Mulla, G. Battaglia, C. Smythe, J. A. Thomas, *Chem. Sci.* **2013**, *4*, 4512–4519; d) S. A. Archer, A. Raza, F. Dröge, C. Robertson, A. J. Auty, D. Chekulaev, J. A. Weinstein, T. Keane, A. J. H. M. Meijer, J. W. Haycock, S. Macneil, J. A. Thomas, *Chem. Sci.* **2019**, *10*, 3502–3513.

[7] a) M. Stephenson, C. Reichardt, M. Pinto, M. Wächtler, T. Sainuddin, G. Shi, H. Yin, S. Monro, E. Sampson, B. Dietzek, S. A. McFarland, *J. Phys. Chem. A* **2014**, *118*, 10507–10521; b) C. Reichardt, K. R. Schneider, T. Sainuddin, M. Wächtler, S. A. McFarland, B. Dietzek, *J. Phys. Chem. A* **2017**, *121*, 5635–5644; c) C. Reichardt, T. Sainuddin, M. Wächtler, S. Monro, S. Kupfer, J. Guthmuller, S. Gräfe, S. McFarland, B. Dietzek, *J. Phys. Chem. A* **2016**, *120*, 6379–6388.

[8] a) E. Baggaley, J. A. Weinstein, J. G. Williams, *Coord. Chem. Rev.* **2012**, *256*, 1762–1785; b) V. Fernández-Moreira, F. L. Thorp-Greenwood, M. P. Coogan, *Chem. Commun.* **2010**, *46*, 186–202; c) D. L. Ma, H. Z. He, K. H. Leung, D. S. H. Chan, C. H. Leung, *Angew. Chem. Int. Ed.* **2013**, *52*, 7666–7682; *Angew. Chem.* **2013**, *125*, 7820–7837; d) F. L. Thorp-Greenwood, R. G. Balasingham, M. P. Coogan, *J. Organomet. Chem.* **2012**, *714*, 12–21.

[9] D. Davydova, A. de la Cadena, D. Akimov, B. Dietzek, *Laser Photonics Rev.* **2016**, *10*, 62–81.

[10] K. R. A. Schneider, A. Chettri, H. D. Cole, K. Reglinski, J. Brückmann, J. A. Roque, A. Stumper, D. Nauroozi, S. Schmid, C. B. Lagerholm, S. Rau, P. Bäuerle, C. Eggeling, C. G. Cameron, S. A. McFarland, B. Dietzek, *Chem. Eur. J.* **2020**, *26*, 14844–14851.

[11] S. A. McFarland, N. S. Finney, *J. Am. Chem. Soc.* **2002**, *124*, 1178–1179.

[12] a) M. K. Kuimova, *Phys. Chem. Chem. Phys.* **2012**, *14*, 12671–12686; b) F. Ricchelli, *J. Photochem. Photobiol. B* **1995**, *29*, 109–118.

[13] a) E. M. Grumstrup, M. M. Gabriel, E. E. Cating, E. M. Van Goethem, J. M. Papanikolas, *Chem. Phys.* **2015**, *458*, 30–40; b) Y. Zhu, J.-X. Cheng, *J. Chem. Phys.* **2020**, *152*, 020901.

[14] T. Yang, A. Chettri, B. Radwan, E. Matuszyk, M. Baranska, B. Dietzek, *Chem. Commun.* **2021**, *57*, 6392–6395.